Iraqi Journal of Physics, 2023 *Vol. 21 No. 4, PP. 45-55*
https://doi.org/10.30723/ijp.v21i4.1148
P-ISSN: 2070-4003
E-ISSN: 2664-5548

Characterization of Magnetized-Plasma System Induced by Laser

Zahraa Marid Abbas[1a*] and Qusay Adnan Abbas[1b]
[1]*Department of Physics, College of Science, University of Baghdad, Baghdad, Iraq*
[b]E-mail: qusay.a@sc.uobaghdad.edu.iq
[a*]Corresponding author: zahraamarid92@gmail.com

Abstract

This study investigated the effect of applying an external magnetic field on the characteristics of laser-induced plasma, such as its parameters plasma, magnetization properties, emission line intensities, and plasma coefficients, for plasma induced from zinc oxide: aluminum composite (AZO) at an atomic ratio of 0.3 wt%. Plasma properties include magnetization and emission line intensities. The excitation was done by a pulsed laser of Nd:YAG with 400 mJ energy at atmospheric pressure. Both the electron temperature and number density were determined with the help of the Stark effect principle and the Boltzmann-Plot method. There was a rise in the amount of (n_e) and (T_e) that was produced by applying a magnetic field and, on the other hand, using the 532 nm wavelength rather than the fundamental wavelength of a laser. The emission lines in the atmosphere's plasma have an appearance of Lorentzian shape. The 532 nm laser exhibited a decrease in both the Larmor radius and the confinement factor compared with the 1064 nm laser. By applying the magnetic field, the Laser Induced Breakdown Spectroscopy (LIBS) intensities increased by 1.44 times when compared to the emissions before applying the field. In addition, the spectral line intensities improved with the fundamental wavelength compared to the second harmonic frequency as a result of the increase in the extracted materials. This is due to the increase in the absorbance of the laser by the target, as some of these materials are excited, so they act as emission sources, which makes them more detectable.

Article Info.

Keywords:
LIBS, Diagnostics, ZnO, Magnetized, Laser.

Article history:
Received: Jun. 16,2023
Revised: Sep. 06, 2023
Accepted: Sep. 28, 2023
Published:Dec. 01,2023

1. Introduction

Laser-induced breakdown spectroscopy (LIBS) is an analytical method that employs the emitted spectra from plasma induced by a pulsed laser from a sample surface [1]. Recently, LIBS has become increasingly in use in numerous fields and in a variety of applications [2, 3]. This can be attributed to its capacity for use to analyze small specimens, real-time detection, ease of use, and remote detection [4, 5]. LIBS has become increasingly popular in recent years and has found widespread application in a variety of fields [6]. It is also attached to devices that are simple to handle and relatively inexpensive [7, 8]. Utilizing lasers with varied targets can perform an analysis of the sample's constituents in real-time, which is referred to as online analysis [9]. Applications of LIBS have now spread to numerous fields for elemental composition determination of products [10], biomedical applications [11], environmental applications [12], geological studies [13], and mineral mining process control [14].

In LIBS, the plasma processes are highly related to the surrounding media [15, 16], in addition to the laser parameters [17]. LIBS is also affected by many factors, such as the pressure of the surrounding media [18], and laser wavelength [19]. The interaction capability of the used laser to induce plasma as well as the confinement effect can lead to an increase in both plasma density and the emission signal detectability [20].

The average temperature of the electrons, denoted by T_e, and the plasma density,

denoted by n_e, are the two most important parameters that determine the properties of plasma [21-23]. The intensity of electronic transition changes obeys the Boltzmann distribution principle according to the plasma temperature (T_e), the transition probability (A_{ji}) of the detected line, and the statistical weight (g_j) of its upper level, as presented by the formula [24].

$$I_{ji} = \frac{N}{U(T)} g_j A_{ji} h\upsilon_{ji} e^{-E_j/k_\beta T_e} \quad (\mathbf{1})$$

where E_j is the upper-level energy, k_B is the Boltzmann constant, and $U(T)$ represents the partition function. This relationship can be rewritten in the form of a Boltzmann-Plot [25], which is utilized in the calculations of electron temperature [26, 27]:

$$\ln\left[\frac{\lambda_{ji} I_{ji}}{hcA_{ji} g_j}\right] = -\frac{1}{kT}(E_j) + \ln\left|\frac{N}{U(T)}\right| \quad (\mathbf{2})$$

where λ_{ji} is the wavelength of emitted line, and N_j is the number density. A linear plot of $\ln\left[\frac{\lambda_{ji} I_{ji}}{hcA_{ji} g_j}\right]$ versus (E_j) has a slope equals to the inverse of plasma temperature [28].

The relationship can be employed to determine the electron number density in accordance with the Stark broadening effect [29, 30].

$$n_e = \left(\frac{\Delta\lambda_{FWHM}}{2\omega}\right) \times N_r \quad (\mathbf{3})$$

where $\Delta\lambda_{FWHM}$ is the instrument broadening subtracted from the emitted line width, ω is the electron impact factor, and N_r is the reference electron density [31].

If any external fields were applied, the plasma insulated itself for a brief distance corresponding to the plasma's size. The Debye-length (λ_D) is the sheath thickness beyond which the electric field is shielded [32, 33].

$$\lambda_D = \sqrt{\frac{\varepsilon_0 k_B T_e}{n_e e^2}} \quad (\mathbf{4})$$

where e represents the charge carried by an electron and ε_0 represents the permittivity of an empty space. The first criterion for plasma is $L >> \lambda_D$ that its geometrical size, denoted by L, must be much greater than λ_D.

The second criterion for plasma is the existence of large number of electrons inside the "Debye sphere" in order to satisfy the collective behaviour [34, 35]:

$$N_D = \frac{4\pi n_e}{3} \lambda_D^3 \gg 1 \quad (\mathbf{5})$$

According to the third criterion, the electromagnetic forces that dominate the movements of the particles must be stronger than their collisional actions. The plasma frequency, often known as the electron oscillation frequency, is equal to [36]:

$$\omega_p = 2\pi f_p = \sqrt{\frac{n_e e^2}{m_e \varepsilon_0}} \quad (\mathbf{6})$$

Laser-induced plasma can be confined by different techniques to enhance the plasma breakdown, such as magnetic confinement by applying an external field [37, 38],

changing the surrounding gas or working pressures, and inertial confinement using dual laser pulses [39].

Atif et al. (2018) [40] investigated what happened to LIBS when they applied an external field at various working pressures using nano-pulsed of Nd: YAG laser while the chamber was filled with helium and argon gases. It was noted that the external field and the conditions of the ambient gas have a significant impact on the emission line intensities as well as the plasma parameters. When the magnetic confinement was increased to higher levels, there was a corresponding increase in the electron number density at all of the different pressures.

During the process of preparing AZO thin films using PLD, Reason et al. (2020) [41] investigated the effect of the presence of various kinds of gas backgrounds at varying pressures on the formation of plasma by a 355 nm laser. The findings of the OES measurements revealed that the intensities of the emitted lines of the species in O_2 and Ar first experience a slight decrease and then go on to experience an exponential increase above a pressure of -5 Pa.

In this study, a full description of the influence of an external magnetic field and laser wavelength on the laser-induced breakdown characteristics was presented.

2. Methodology

A mixture of zinc oxide (ZnO) and aluminum (Al) with atomic ratios of 0.3 wt% is compressed in a mold made of stainless steel at a pressure of 5 torr for 15 min in order to create a target for LIBS. This process occurred in a stainless-steel mold to produce capsules with a diameter of 1 cm. In order to successfully finish the process, a pulsed Nd: YAG laser at two different wavelengths (1064 and 532 nm) was utilized. The laser works with a spot diameter of 2 mm, pulse duration of 9 ns, pulse energy of 400 mJ, and falls perpendicularly on the target. The optical fiber was set to make 45° with the target surface at a distance of 5 cm from the laser spot. The breakdown was helped in its progression by a permanent magnet that was positioned behind the target of a magnetic field that was 77.2 mT. The emissions of the plasma plume were analyzed using a wide-range spectrometer (Thorlabs- CCS 100/M) with a spectral resolution of 0.1 nm and a wavelength range of 300-800 nm. All of the tests were performed at the standard atmosphere pressure (Fig. 1).

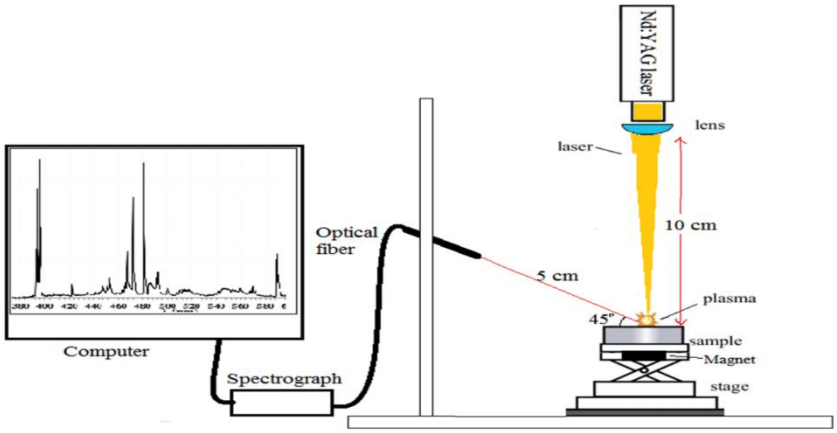

Figure 1: The schematic diagram of the LIBS configuration.

3. Results and Discussion

Figs. 2 and 3 display a comparison between the spectroscopic patterns of LIBS in atmosphere from the AZO composite without and with applying the magnetic field, using the fundamental and second-order frequencies of laser, respectively. According to

the information that was provided by the National Institute of Standards and Technology (NIST), the lines of the appeared emission peak were matched with the emission lines of atomic and ionic zinc and aluminium species (Zn-I, Al-I, Zn-II, and Al-II) [42]. This finding is possible because of the fact that zinc and aluminium are both elements that can exist in both atomic and ionic forms. Different wavelengths showed different patterns which have varied intensities due to the fact that the probabilities of the various transitions, as well as the statistical weight that is assigned to each transition, are responsible for these variations. Because plasma has a low ionization degree, the intensity of emitted lines from atomic species is significantly higher than that ionic ones indicated on low degree of ionization [43]. The Zn emission lines in the spectrum appeared to have a higher intensity than the Al emission lines, which can be attributed to the different amounts of these elements that were present in the target. Because of the magnetic confinement effect, the intensity of the emission lines which were observed by LIBS increased when an external magnetic field was present. This is because the magnetic confinement both inhibits and slows the expansion of plasma. After the removal of excitation from the atoms that were excited by the laser, the species that were confined to a limited space that had a high temperature and density acted as emission sources [44]. Applying the magnetic field caused a significant broadening of the spectral lines observed in the atmospheric air, and the lines continued to become more diffuse as the magnetic field was used. According to Stark's phenomena, the emission lines broaden as the electron density rises, which indicates that the magnetic confinement has a significant effect [45].

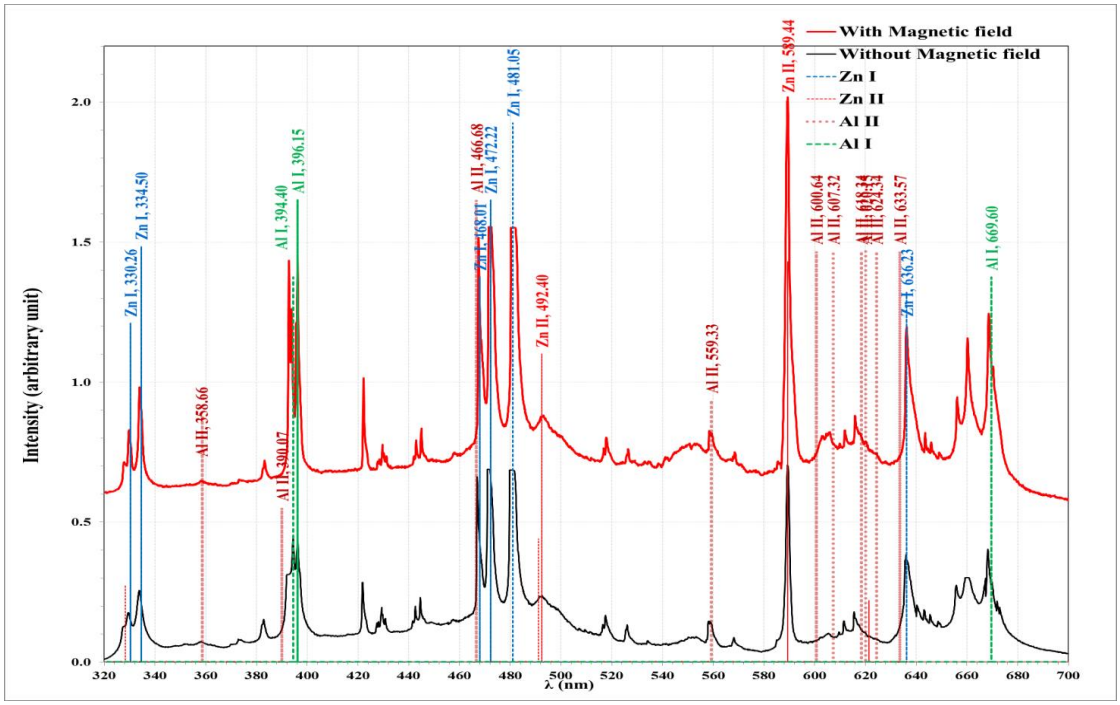

Figure 2: LIBS for AZO target in atmospheric air without and with magnetic field using 1064 nm Laser.

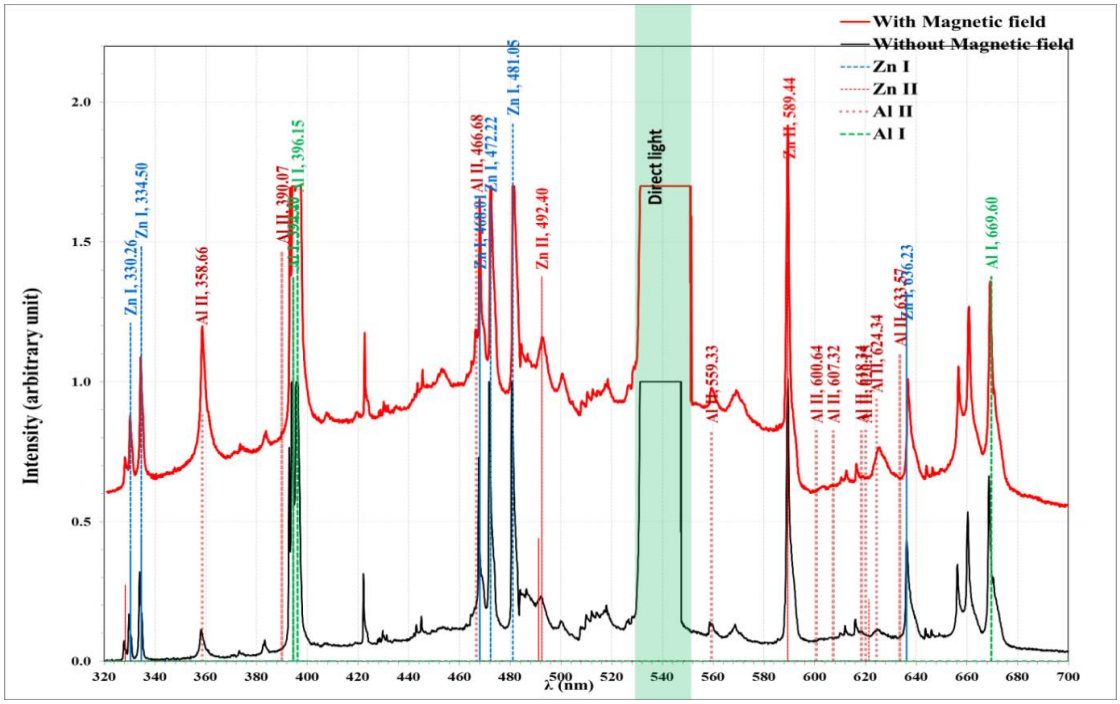

Figure 3: LIBS for AZO target in atmosphere air without and with the presence of magnetic field using 532 nm laser.

Emission lines which were produced by lasers with a wavelength of 1064 nm appeared higher than 532 nm for the same power. The interaction between the 532 nm wavelength and the target less due to less absorption of the surface. A higher photon energy that has the same laser power contains fewer photons that produce a lower amount of ablated materials that act as emission sources [46].

In addition, there is a neglected region in which the direct reflection of green laser light appears with high intensity. This range of wavelengths cannot be used in the analysis of the LIBS spectra.

Table 1 displays the difference in LIBS intensity of the Zn-I (481 nm) emission line in the air using the two different laser wavelengths. This comparison was performed without and with the magnetic field. It was noted that the line intensity for plasma that was induced by the magnetic field from the AZO target was approximately 1.44 times higher than that observed when there was no magnetic field. This observation is due to the intricate interplay between the magnetic field and the plasma dynamics. When the magnetic field is applied, it exerts a confining influence on the plasma plume generated during the laser ablation process [47]. The length of the plasma plume is inhibited by the magnetic field leading to a shorter and more focused plume. This confinement leads to a more concentrated and structured expansion of the plasma, resulting in an increased density of excited plasma species within a confined volume. Furthermore, the presence of the magnetic field enhances collisional processes within the plasma, promoting more efficient excitation of atoms and ions to higher energy states [48]. As a consequence, a greater population of excited species is available to emit characteristic wavelengths of light during the return to lower energy states. The interactions between the magnetic field and the charged particles within the plasma likely lead to altered trajectories and energy distributions [49]. These effects can affect the spatial distribution of the emitting species and modify the kinetics of the emission process [50]. As a result, the characteristic emission lines became more pronounced and exhibited higher intensities in the presence of the magnetic field. Additionally, the LIBS intensity significantly increased in its emission intensity at the 1064 nm laser associated

with the 532 nm as a result of more ablated matter using the fundamental wavelength [51]. This was a result of the fact that the fundamental wavelength was used.

Table 1: Zn-I (481 nm) emission line intensity in arbitrary units for the two laser wavelength (1064 and 532 nm) without and with magnetic field.

Magnetic field	**Laser wavelength (nm)**	
	1064	532
Without magnetic field	0.55	0.36
With magnetic field	0.80	0.52

Fig. 4 illustrates the Zn-I 481 nm emission line profiles with the best Lorentzian fit in the two cases without and with the external field for the two laser wavelengths. The line broadening increased after applying the external field. This is accomplished by limiting the expansion of the plasma plume, which in turn causes the ne to increase, giving the appearance that the line profile is broadening [52]. The n_e was determined according to Stark broadening effect (Eq. (1)).

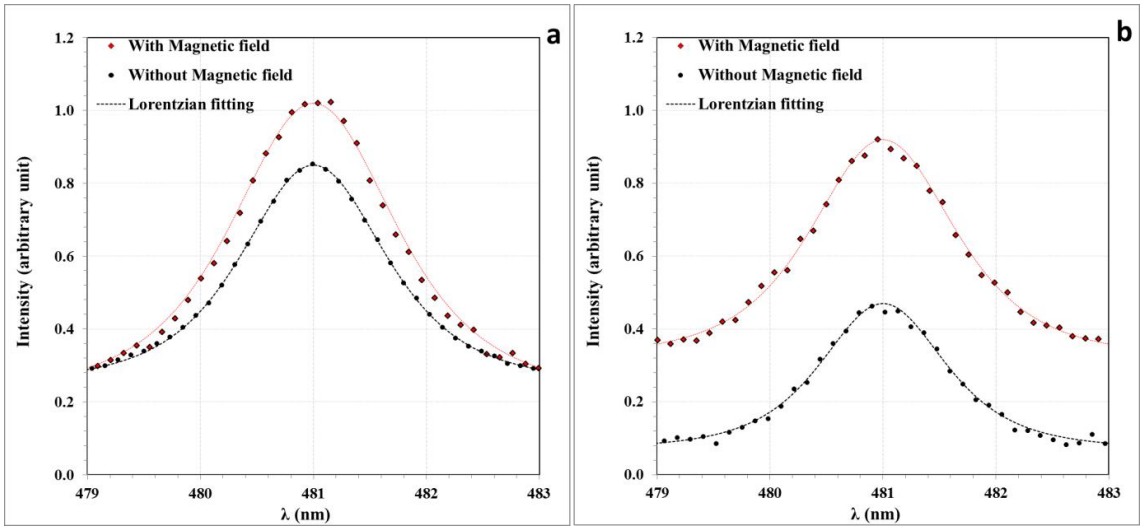

Figure 4: Zn-I 481 nm line profiles and its Lorentzian fitting in air before and after applying external field using 1064 nm (a), and 532 nm (b) laser wavelengths.

Fig. 5 and 6, show how the Boltzmann-Plot (Eq. (2)) was employed to calculate the electron temperature (T_e) for the two wavelengths of laser. This was done with Al-I standard lines from NIST, which are listed in Table 2. This was done with and without magnetic field.

Table 3 provides a comparison of the values of T_e and n_e without and with the external field, and their variation with the change in laser wavelength. Because of the magnetic confinement effect of the plasma generated after breakdown on the target surface, it is abundantly clear that both T_e and ne increased when there is an external field. Active electrons and other types are able to travel further distances before their energy is depleted as a result of inelastic collisions [53]. The magnetic field exerts a constraining force on the expansion of the plasma column, which results in an increase in ne. Because less energy was transferred from the laser beam to the plasma plume when using the 532 nm laser instead of the 1064 nm one, both T_e and ne were slightly reduced when the breakdown was produced. This is in contrast to the results obtained when using the 1064 nm laser [54, 55].

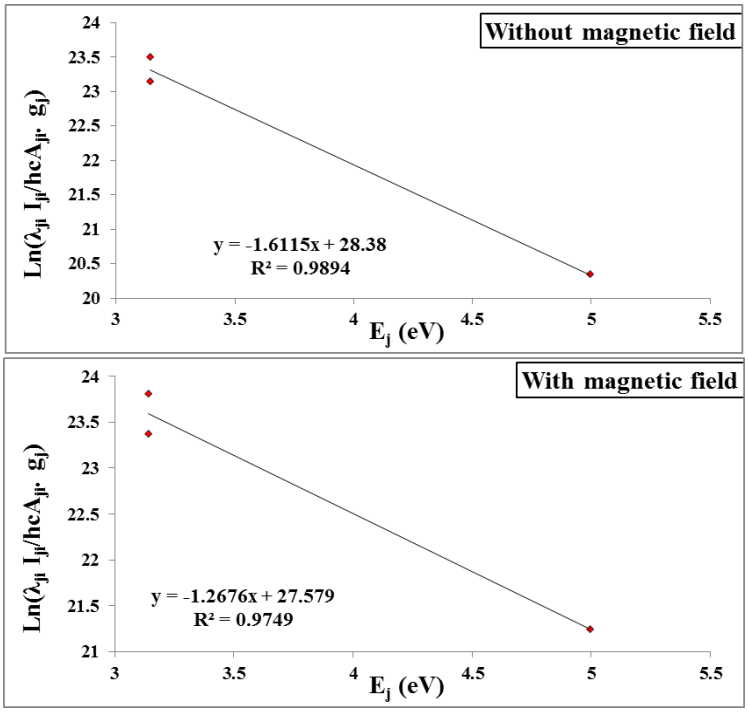

Figure 5: Boltzmann-plot for Al-I lines for the LIBS using 1064 nm laser without and with external field.

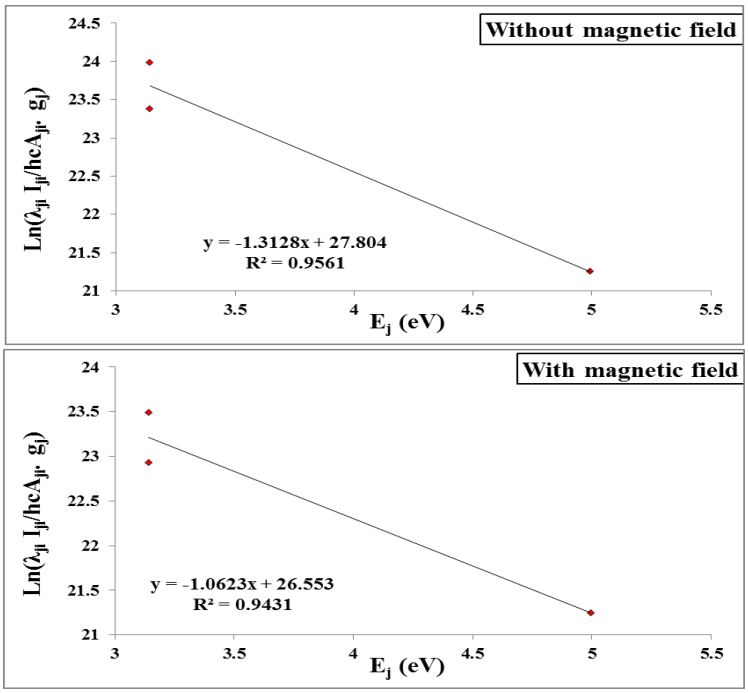

Figure 6: Boltzmann-plot for Al-I lines for the LIBS using 532 nm laser without and with magnetic field.

Table 2: The NIST data for the selected Al-I lines that used in Boltzmann-Plot.

λ (nm)	$A_{ji}.g_j \times 10^7$	Lower level (eV)	Upper level (eV)
394.40	9.98	0.00	3.14
396.15	19.70	0.01	3.14
669.60	0.40	3.14	4.99

Table 3: plasma parameters for plasma induced in air using 1064 and 532 nm laser wavelengths without and with external field.

Laser wavelength (nm)	E (mJ)	T_e (eV)	FWHM (nm)	$n_e \times 10^{18}$ (cm^{-3})	$f_p \times 10^{12}$ (Hz)	$\lambda_D \times 10^{-6}$ (cm)	N_D
1064	Without	0.762	1.50	0.455	6.054	9.619	1694
	With	0.941	1.70	0.515	6.445	10.044	2186
532	Without	0.621	1.30	0.394	5.636	9.325	1338
	With	0.789	1.50	0.455	6.054	9.788	1786

Significant variations in plasma characteristics with the magnetic effect were observed in atmosphere with increasing plasma frequency, Debye length, and Debye number, especially with 1064 nm wavelength. This region also has the highest electron number density and the lowest electron temperature [56]. The significant effect that an external magnetic field has on the plasma number density and the relation that this effect has with the other parameters, the plasma frequency values have a tendency to behave in the same manner as n_e, which is to say that they were increased in the magnetic field. This is due to the plasma number density's obvious confinement impact by the external field, which is connected to other plasma properties [57]. These two components had a direct impact on the considerable increase in T_e, D, and ND, which both rose T_e [58].

Larmor radius for electron gyration is determined by

$$r_L = \frac{v}{\omega_c} = \frac{m_e v}{q\,B} \qquad (7)$$

where v represents the thermal velocity and ω_c is the cyclotron frequency.

Table 4 provides Larmur radius and β factor for the two-laser wavelength the electrons' gyration. The application of the magnetic field using the two different wavelengths has resulted in the formation of this radius. Because the radius of Larmor in a magnetic field that is held constant is directly related to the velocity of electrons (which is related to their temperature), the use of a laser with a wavelength of 532 nm results in a slight increase in r_L. One way to determine whether or not the concept of magnetic confinement holds water is to calculate the magnetic confinement factor β. In this case, thermal beta is understood to be the ratio of plasma pressure to magnetic pressure. The plasma induced by both laser wavelengths of $\beta < 1$, which indicates that magnetic confinement is functioning effectively [59]. The β value less than one is due to the fact that the magnetic pressure is greater than the plasma pressure. Plasma that was produced by a laser with a wavelength of 532 nm experienced an increase in β value, which can be interpreted as a decrease in the efficiency of magnetic confinement. The efficiency of the confinement at 532 nm decreases as a direct result of the high number of collisions that are occurring in the system. It would seem that changing the laser's wavelength would be a useful way to affect the values that atmospheric LIBS measures in the desired way. The observed decrease in both the Larmor radius and the confinement factor for the 532 nm laser, when compared with the 1064 nm laser, is a consequence of the higher photon energy and momentum associated with the shorter wavelength. This leads to more pronounced interactions between the laser light and the plasma particles, resulting in altered plasma dynamics and reduced confinement effects within the magnetic field [60].

Table 4: Larmur radius and β factor for the two-laser wavelength.

Laser wavelength (nm)	r_L (mm)	β
1064	0.040	0.29
532	0.038	0.24

4. Conclusions

In this study, we examined the impact of magnetic confinement, facilitated by a simple magnet configuration, and the influence of laser wavelength on the plasma generated from Al doped ZnO (AZO) target, with a focus on its applicability for LIBS. The investigation yielded several noteworthy findings. First of all, employing a permanent magnet resulted in a discernible enhancement of LIBS performance. Specifically, the electron number density (n_e) exhibited an increase attributed to heightened inelastic collisions, stemming from the constraint imposed on plasma expansion by the magnetic field. Simultaneously, the electron temperature (T_e) experienced an elevation under the influence of the magnetic field, attributed to the delay in energy dissipation resulting from controlled plume expansion. From analysing the spatial characteristics of the plasma, it was observed that the Larmor radius, which signifies the gyration radius of charged particles in the magnetic field along with the confinement factor β, displayed a reduction when employing a laser with a second harmonic wavelength (532 nm). This decrease in Larmor radius and confinement factor indicates a relatively diminished effect of magnetic confinement compared to the fundamental wavelength (1064 nm) of the laser. This investigation elucidated the beneficial impact of magnetic confinement through a simple magnet configuration on the plasma generated from an AZO target for LIBS applications. The utilization of a magnetic field resulted in improved electron number density, elevated electron temperature, and intensified emission line intensities. Furthermore, the intricate interplay between laser wavelength and magnetic field revealed nuanced effects on plasma spatial characteristics, offering valuable insights for advancing LIBS techniques and enhancing their analytical capabilities.

Conflict of Interest

Authors declare that they have no conflict of interest.

References

1. J. C. Lindon, G. E. Tranter, and D. Koppenaal, *Encyclopedia of Spectroscopy and Spectrometry* (San Diego, USA, Academic Press, 2016).
2. M. Alhamadani, Iraqi J. Phys. **21**, 68 (2023).
3. A. Hussein and H. M. Abdullah, Iraqi J. Phys. **21**, 58 (2023).
4. S. K. H. Shah, J. Iqbal, P. Ahmad, M. U. Khandaker, S. Haq, and M. Naeem, Rad. Phys. Chem. **170**, 108666 (2020).
5. J. Peng, F. Liu, F. Zhou, K. Song, C. Zhang, L. Ye, and Y. He, Tren. Analyt. Chem. **85**, 260 (2016).
6. A. L. Abed and M. T. Hussein, Iraqi J. Phys. **20**, 53 (2022).
7. D. W. Hahn and N. Omenetto, Appl. Spectro. **66**, 347 (2012).
8. M. M. Manhil and R. K. Jamal, Iraqi J. Phys. **21**, 44 (2023).
9. M. Rühlmann, D. Büchele, M. Ostermann, I. Bald, and T. Schmid, Spectrochim. Acta Part B: Atom. Spectro. **146**, 115 (2018).
10. A. Ahmed, M. Salman, M. Alwazzan, and A. Meri, J. Adv. Res. Dynam. Cont. Sys. **2**, 1 (2019).

11. Z. L. Petrović, N. Puač, S. Lazović, D. Maletić, K. Spasić, and G. Malović, in Journal of Physics: Conference Series (IOP Publishing, 2012). p. 012001.
12. Y. Zhang, T. Zhang, and H. Li, Spectrochim. Acta Part B: Atom. Spectro. **181**, 106218 (2021).
13. S. N. P. Panya, A. Galmed, M. Maaza, B. Mothudi, and M. Harith, Mat. Today: Proce. **36**, 600 (2021).
14. A. K. Myakalwar, C. Sandoval, M. Velásquez, D. Sbarbaro, B. Sepúlveda, and J. Yáñez, Minerals **11**, 1073 (2021).
15. A. F. Rauuf and K. A. Aadim, Iraqi J. Sci. **64**, 2877 (2023).
16. G. M. Jassam and S. S. Ahmed, Iraqi J. Phys. **21**, 91 (2023).
17. I. Urbina, F. Bredice, C. Sanchez-Aké, M. Villagrán-Muniz, and V. Palleschi, Spectrochim. Acta Part B: Atom. Spectro. **195**, 106489 (2022).
18. S. Amoruso, R. Bruzzese, X. Wang, and J. Xia, Appl Phys. Lett. **92**, 041503 (2008).
19. Q. A. Abbas, Iraqi J. Sci. **60**, 1251 (2019).
20. D. Bradley, C. Sheppard, I. Suardjaja, and R. Woolley, Comb. Flame **138**, 55 (2004).
21. Y. Ohtsu and K. Kihara, IEEE Trans. Plasma Sci. **40**, 1809 (2012).
22. G. H. Jihad and K. A. Aadim, Iraqi J. Sci. **63**, 2039 (2022).
23. S. E. Abdulghani and Q. A. Abbas, Iraqi J. Sci. **64**, 2297 (2023).
24. D. Devia, L. Rodriguez-Restrepo, and E. R. Parra, Ingen. Y Cienc. **11**, 239 (2015).
25. S. Hamed, Egypt. J. Sol. **28**, 349 (2005).
26. A. K. Abd and Q. A. Abbas, Iraqi J. Sci. **64**, 2867 (2023).
27. V. Unnikrishnan, K. Alti, V. Kartha, C. Santhosh, G. Gupta, and B. Suri, Pramana **74**, 983 (2010).
28. Z. Farooq, R. Ali, U. S. Qurashi, M. H. Mahmood, M. Yaseen, M. A. Qayyum, M. N. Hussain, S. M. Shah, and T. Jan, Phys. Plasm. **25**, 093106 (2018).
29. X.-F. Li, W.-D. Zhou, and Z.-F. Cui, Fron. Phys. **7**, 721 (2012).
30. T. A. Hameed, H. R. Humud, and L. F. Ali, Iraqi J. Sci. **64**, 2889 (2023).
31. M. S. Dimitrijević and S. Sahal–Bréchot, Astron. Astrophys. Suppl. Ser. **140**, 193 (1999).
32. G. Petraconi, A. G. Neto, H. Maciel, and R. Pessoa, in Journal of Physics: Conference Series (IOP Publishing, 2012). p. 012041.
33. I. K. Abbas and K. A. Aadim, Iraqi J. Sci. **64**, 2271 (2023).
34. A. L. Winfrey, M. A. Abd Al-Halim, J. G. Gilligan, A. V. Saveliev, and M. A. Bourham, IEEE Transact. Plasma Sci. **40**, 843 (2012).
35. A. Dinklage, T. Klinger, G. Marx, and L. Schweikhard, *Plasma Physics: Confinement, Transport and Collective Effects* (Greifswald, Germany, Springer Science & Business Media, 2005).
36. C. Fallon, Thesis, Dublin City University, 2013.
37. Y. Lu, C. Yang, H. Wang, L. Ma, M. Xu, and L. Xi, Vacuum **211**, 111912 (2023).
38. Z. M. Abbas and Q. Adnan, Iraqi J. Sci. **61**, 341 (2020).
39. A. Hussain, G. Xun, H. Asghar, M. Azam, Q.-T.-. Ain, and Z. Nawaz, Opt. Spectros. **129**, 452 (2021).
40. A. Hussain, M. Tanveer, G. Farid, M. B. Hussain, M. Azam, and W. Khan, Optik **172**, 1012 (2018).
41. K. Reeson, S. L. Yap, S. F. Koh, C. H. Nee, T. Y. Tou, and S. S. Yap, Th. Sol. Fil. **701**, 137953 (2020).
42. Y. Ralchenko. *NIST Atomic Spectra Database*; https://www.nist.gov/pml/atomic-spectra-database.
43. N. Bolouki, J.-H. Hsieh, C. Li, and Y.-Z. Yang, Plasma **2**, 283 (2019).

44. F. Bredice, P. P. Martinez, C. Sánchez-Aké, and M. Villagrán-Muniz, Spectrochim. Acta Part B: Atom. Spectro. **107**, 25 (2015).
45. A. F. Ahmed, F. a.-H. Mutlak, and Q. A. Abbas, Appl. Phys. A **128**, 147 (2022).
46. H. Imran, K. Hubeatir, and K. Aadim, Eng. Tech. J. **40**, 1307 (2022).
47. M. S. J. Hashmi, *Comprehensive Materials Processing* (USA, Newnes, 2014).
48. A. Dawood, S. Bashir, N. A. Chishti, M. A. Khan, and A. Hayat, Laser Par. Beams **36**, 261 (2018).
49. P. Shustov, A. Artemyev, and E. Yushkov, Phys. Lett. A **379**, 590 (2015).
50. G. Ganguli, C. Crabtree, A. Fletcher, and B. Amatucci, Rev. Mod. Plasma Phys. **4**, 1 (2020).
51. V. N. Rai, H. Zhang, F. Y. Yueh, J. P. Singh, and A. Kumar, Appl. Opt. **42**, 3662 (2003).
52. Z. Hao, Z. Deng, L. Liu, J. Shi, and X. He, Front. Optoelect. **15**, 17 (2022).
53. J. Weng, S. Kashiwakura, and K. Wagatsuma, Analyt. Sci. **37**, 367 (2021).
54. N. Glumac and G. Elliott, Opt. Laser Eng. **45**, 27 (2007).
55. Z. A. Abbas and Q. A. Abbas, in AIP Conference Proceedings (AIP Publishing, 2021). p.
56. H. M. Fadhil, K. I. Hassoon, and H. A. Salih, J. Appl. Sci. Nanotech. **2**, 85 (2022).
57. M. Mahmoodi-Darian, M. Ettehadi-Abari, and M. Sedaghat, J. Theo. Appl. Phys. **10**, 33 (2016).
58. N. S. J. Braithwaite, Plasma Sour. Sci. Tech. **9**, 517 (2000).
59. M. A. Khan, S. Bashir, N. A. Chishti, E. Bonyah, A. Dawood, and Z. J. a. A. Ahmad, AIP Advan. **13**, 015017 (2023).
60. P. K. Pandey and R. Thareja, J. Appl. Phys. **109**, 074901 (2011).

توصيف نظام البلازما الممغنطة الناجم عن الليزر

زهراء مارد عباس[1] و قصي عدنان عباس[1]

[1]قسم الفيزياء، كلية العلوم، جامعة بغداد، بغداد، العراق

الخلاصة

في هذه الدراسة، تم التحقق من تأثير تطبيق مجال مغناطيسي خارجي على خصائص البلازما المستحثة بالليزر، مثل معلماتها وخصائص المغنطة وشدة خطوط الانبعاث، ومعاملات البلازما المستحثة من هدف مزيج أكسيد الزنك: ألمنيوم (AZO) وبالنسبة 0.3٪ بالوزن. تم الإثارة بواسطة ليزر Nd: YAG النبضي ذو طاقة 400 مللي جول في الضغط الجوي. تم تحديد كل من درجة حرارة البلازما وكثافتها بمساعدة مبدأ تأثير ستارك وطريقة بولتزمان-بلوت. كان هناك ارتفاع في قيم (n_e) و (T_e) التي تم إنتاجها بوجود مجال مغناطيسي، ومن ناحية أخرى، باستخدام الطول الموجي 532 نانومتر بدلا من الطول الموجي الأساسي لليزر. خطوط الانبعاث في بلازما الغلاف الجوي لها شكل لورنتزيان. أظهر الليزر 532 نانومتر انخفاضًا في كل من نصف قطر لارمور وعامل الحبس المغناطيسي مقارنة بالليزر 1064 نانومتر. زادت شدة LIBS بنحو 1.33 مرة مع تطبيق المجال المغناطيسي مقارنة بالانبعاثات قبل تطبيق المجال. بالإضافة إلى ذلك، تم تحسين شدة الخطوط الطيفية مع الطول الموجي الأساسي مقارنة بالتردد التوافقي الثاني نتيجة الزيادة في المواد المستخرجة نتيجة زيادة امتصاص الليزر بواسطة الهدف، حيث يتم تهييج بعض هذه المواد لذلك فهي تعمل كمصادر انبعاث، مما يجعلها أكثر قابلية للاستكشاف.

الكلمات المفتاحية: LIBS، تشخيص، ZnO، الممغنطة، الليزر.